Dynamics Study of the N(^4S) + O_2 Reaction and Its Reverse

P. J. B. S. Caridade and A. J. C. Varandas*

Departamento de Quimica, Universidade de Coimbra, 3004-535 Coimbra, Portugal

Received: October 9, 2003; In Final Form: December 16, 2003

We report quasiclassical trajectory calculations for the reaction N(^{4}S) + O_2 → NO + O by focusing on the rovibrational distributions of the NO product molecule at a collisional energy of 3 eV and the temperature dependence of the rate constant. The calculations employ the lowest adiabatic sheet of a recently reported (Varandas, A. J. C. *J. Chem. Phys.* **2003**, *119*, 2596) multisheeted double many-body expansion potential energy surface for the $^2A'$ states of NO_2, improved via a multiple energy-switching scheme to attain near-spectroscopic accuracy in the vicinity of the deep $\tilde{X}\ ^2A_1$ minimum. For the quartet state, the calculations employ single-sheeted potentials from various sources, except for the rate constant where the results are taken from the literature. The rate constant for the reverse endothermic reaction is calculated by dividing the rate constant for the forward reaction by the equilibrium constant calculated using statistical mechanics. For both reactions, the agreement with the recommended rate constants is good. The vibrational distributions of NO are found to agree with previously reported theoretical estimates, which show fair agreement with the general trends observed from experiment.

1. Introduction

Highly rovibrationally excited NO molecules are known to play an important role in the earth's atmosphere, being produced by the reaction[1]

$$N(^4S) + O_2 \rightarrow NO + O \quad (1)$$

Such species are responsible for the quiescent daytime[2] and nighttime[3,4] thermospheres and are necessary for an understanding of natural and artificial terrestrial auroras.[5] It is also well established that reaction 1 together with

$$N_2 + O \rightarrow NO + N \quad (2)$$

are the main sources of nitric oxide in combustion processes via the Zeldovich mechanism.[6] Although reaction 1 has a large exothermicity, 1.38 eV, the experimental results[7] indicate the existence of an activation energy of ∼0.3 eV, thus requiring superheated N(^4S) atoms to occur. Such translationally hot atoms are produced by several chemical and/or physical processes[8,9] in the atmosphere, being that their relative lifetimes are large enough to allow reaction before de-excitation through collisions (refs 10 and 11 and references therein) may take place.

The reported studies related to reaction 1 have focused mainly on the vibrational distribution of the products and the temperature dependence of the rate constants. Experimentally, the values of the rate constant for the direct reaction over the temperature range of $298 \le T/\mathrm{K} \le 5000$ were compiled by Baulch et al.,[7] who recommend the expression $k(T) = 1.5 \times 10^{-14} T \exp(-3270/T)\ \mathrm{cm^{-3}\ s^{-1}}$, with $\Delta \log k = \pm 0.12$ for $298 \le T/\mathrm{K} \le 1000$ and $\Delta \log k = \pm 0.3$ for $1000 \le T/\mathrm{K} \le 5000$. In contrast to this rate constant, which is very well defined, the vibrational distribution of the NO(v') product has been a point of some controversy with the appearance of two distinct patterns. The first suggests a declining shape of the population with vibrational quantum number, possibly showing a slight inversion at $v' = 1-2$.[12,13] The other suggests an oscillatory nature for the distribution, but the measurements[14] are difficult to rationalize.

From the theoretical point of view, the reaction is probably the most complicated involving three atoms. The difficulties start with the potential energy surfaces of the $NO_2(^2A')$ system, where the multisheeted nature of the electronic manifold requires a subtle handling at both the calculation and modeling levels. Furthermore, the N(^4S) + $O_2(X\ ^3\Sigma_g^-)$ reactants correlate with three A' surfaces of distinct spin symmetries, namely, $^{2,4,6}A'$. Of these, the doublet state dominates for temperatures below 5000 K or so, and the quartet state gives the major contribution for higher temperatures. Although the sextet state does not correlate with the NO($X\ ^2\Pi$) + O(^3P) products, one still requires at least two electronically adiabatic potential energy surfaces to study the dynamics of the title reaction. The first potential energy surface for $NO_2(^2A')$ was calculated long ago by Walch and Jaffe,[15] and its analytical representation has been performed by Duff et al.[16] using the single-valued many-body expansion[17] (MBE) method. More recently, several other single-valued surfaces of the MBE type have been proposed[18−20] using accurate ab initio data for their calibration. As stated above, such functions cannot reproduce the multisheeted nature of the $^2A'$ electronic manifold, in particular, the well-established $\tilde{X}\ ^2A_1/\tilde{A}\ ^2B_2$ conical intersection that occurs for geometries with C_{2v} symmetry. To encompass such a difficulty, a multisheeted representation has recently been proposed by one of us[21] on the basis of the multivalued double many-body expansion[22−24] (DMBE) formalism. Furthermore, near-spectroscopic accuracy has been conveyed to the lowest adiabatic sheet in the vicinity of the $\tilde{X}\ ^2A_1$ minimum via a multiple energy-switching[25] (ES) scheme. As a result, the lowest adiabatic sheet of such a DMBE/ES potential energy surface is expected to reproduce the main topological features and rovibrational spectra of ground-state NO_2 according to the most up-to-date experimental and theoretical data.

Theoretically, the title reaction has been extensively studied by using the quasi-classical trajectory[16,26−30] (QCT) method, variational transitional-state theory[20,31,32] (VTST), and quantum

* Corresponding author. E-mail: varandas@qtvs1.qui.uc.pt.

10.1021/jp037040k CCC: $27.50
Published on Web 03/18/2004

dynamics,[33−36] which are all based on the lowest electronically adiabatic sheets for the doublet and quartet spin states. Such studies focused on dynamics attributes such as cross sections and vibrational and rotational product distributions as well as specific and thermalized rate constants. Because accurate full-dimensional quantum dynamics calculations are computationally very demanding because of the large number of open channels[36] that are involved, our study will be carried out using the quasi-classical trajectory[37,38] (QCT) method. A realistic sampling procedure will also be employed for O_2, with the major goals being the rovibrational distributions of the NO product molecule and the temperature dependence of the total rate constant for the forward N(^4S) + O_2 exothermic reaction. The rate constant for the reverse reaction will then be estimated from the microreversibility principle by using the rate constant for the direct reaction and the equilibrium constant, which is calculated via statistical mechanics.

The paper is organized as follows. Section 2 provides a brief description of the potential energy surfaces that are employed. The dynamical results for the forward N(^4S) + O_2 reaction are reported in section 3, focusing on the analysis of NO product rovibrational distributions at a fixed collision energy of 3 eV (subsection 3.1) and the thermalized rate constant (subsection 3.2). Section 4 summarizes the results obtained for the O + NO reaction based on the rate constant for the forward reaction and the equilibrium constant. The conclusions are in section 5.

2. Potential Energy Surfaces

The potential energy surface used to describe the lowest $^2A'$ state of NO_2 has been discussed in detail elsewhere,[21] and hence we give here only a brief description of its major features. The basis of such a $^2A'$ surface is the multisheeted DMBE[22−24] method. It starts from the diatomics-in-molecules (DIM) formalism (refs 39 and 40 and references therein) in which a minimal atomic basis set is employed for O(^3P_g) and N(^4S_u). To account for the finite size of the basis sets as well as the missing many-center terms and orbital overlap, a corrective term is introduced in each element of the Hamiltonian matrix, yielding the general form[24]

$$\mathbf{H} = \mathbf{H}^{AB}(\mathbf{1} + \mathbf{F}^{AB}) + \mathbf{R}^{BC}\mathbf{T}^{BC}\mathbf{H}^{BC}(\mathbf{1} + \mathbf{F}^{BC})\,\mathbf{T}^{BC\dagger}\mathbf{R}^{BC\dagger} + \mathbf{R}^{AC}\mathbf{T}^{AC}\mathbf{H}^{AC}(\mathbf{1} + \mathbf{F}^{AC})\,\mathbf{T}^{AC\dagger}\mathbf{R}^{AC\dagger} - \mathbf{H}^{A} - \mathbf{H}^{B} - \mathbf{H}^{C} \quad (3)$$

where **1** is an identity matrix, $\mathbf{H}^{XY}$ is the XY diatomic term, and $\mathbf{H}^{X}$ is the diagonal energy matrix for atom X. In turn, $\mathbf{R}^{XY}$ and $\mathbf{T}^{XY}$ are the rotational and spin-recoupling matrices, and $\mathbf{F}^{XY}$ is a dressing matrix that accommodates the three-body energy terms. The adjustable parameters available in the dressing matrix have in the present case been calibrated using both theoretical and experimental data. With the above-mentioned minimal basis set, the resulting Hamiltonian matrix is 8 × 8. All input diatomic potential curves[21,22] have been represented by using the extended Hartree−Fock approximate correlation energy[41,42] (EHFACE2U) model. The lowest adiabatic surface has subsequently been improved by merging it with an effective spectroscopically accurate polynomial form[43] via the ES[25] scheme. In fact, to allow the narrow energy window for the transition between the two merged surfaces to occur, a novel multiple ES[21] method has been employed. Assuming that the changes in the DMBE/ES (for brevity, this will be denoted simply by the superscript ES) surface are minimal relative to the original DMBE form, the corresponding diabatic matrix may be obtained by back transformation as[44]

$$\mathbf{W}^{ES} = \mathbf{U}\mathbf{V}^{ES}\mathbf{U}^{\dagger} \quad (4)$$

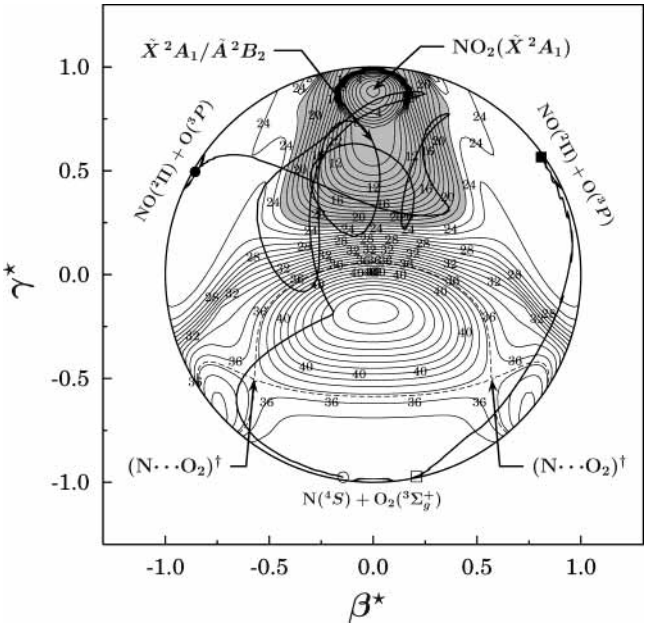

Figure 1. Relaxed triangular plot[45] for the $1^2A'$ electronically adiabatic sheet of the 8 × 8 DMBE/ES[21] potential energy surface. The contours start at $-0.360E_h$, equally spaced by 5 mE_h. Shown by dashed line is the contour associated with the barrier height for the N(^4S) + O_2 reaction. Two sample trajectories (starting at the open symbols and ending at the corresponding filled ones) are also shown: one forms a "complex" (shaded area), and the other is direct. Also indicated is the $\tilde{X}\,^2A_1/\tilde{A}\,^2B_2$ conical intersection.

TABLE 1: Geometric and Energetic Attributes of the Saddle Points on the Lowest Doublet and Quartet Spin-State Surfaces of Relevance for the Title Reaction[a]

surface	R_{NO}/ a_0	R_{OO}/ a_0	∠NOO/ deg	ΔV_b^b/ eV	ω_1/ cm^{-1}	ω_2/ cm^{-1}	ω_3/ cm^{-1}
DMBE[21] ($^2A'$)	3.107	2.513	113.5	0.276	1117.4	461.6	488.5i
MBE[16,46] ($^4A'$)	3.427	2.328	106.8	0.647	1415.7	393.7	306.8i
MBE[20] ($^4A'$)	3.457	2.347	100.6	0.548	1359.5	379.7	563.5i
MBE[20c] ($^4A'$)	2.202	5.456	115.7	−1.445	2020.5	174.5	129.2i

[a] Also shown are the corresponding harmonic vibrational frequencies (symmetric stretching ω_1, bending ω_2, and asymmetric stretching ω_3. [b] Classical barrier height for the N(^4S) + O_2 → NO + O reaction. [c] Saddle point close to the products channel; see the text.

where **U** is the orthogonal matrix that diagonalizes the original DMBE potential matrix. It is the lowest sheet resulting from the diagonalization of the DMBE/ES diabatic potential matrix that will be used for the dynamics studies reported in the present work. Such an adiabatic potential energy surface is shown in Figure 1 as a relaxed triangular plot by using hyperspherical coordinates.[45] Visible from it are the C_{2v} minimum at $\beta^* = 0$ associated with the chemically stable NO_2 molecule and the $\tilde{X}\,^2A_1/\tilde{A}\,^2B_2$ conical intersection ($\beta^* = 0$ and $\gamma^* = 0.757$), which lies 9759 cm^{-1} above the absolute minimum. Also seen are the two equivalent barriers for the N + O_2 reaction that are located at a C_s geometry (this is numerically defined in Table 1) with a barrier height of 0.276 eV. Although the saddle-point geometry has a slightly shorter O−O bond distance than the one predicted from ab initio calculations (see ref 21 and references therein), such a feature should not drastically affect the results reported in the present work, as indeed seems to be the case by comparison with available theoretical and experimental data.

Two potential energy surfaces have been employed for the dynamics calculations carried out on the lowest $^4A'$ state of NO_2, both of which are based on a single-valued MBE[17] representation of the potential energy. They are illustrated as relaxed triangular

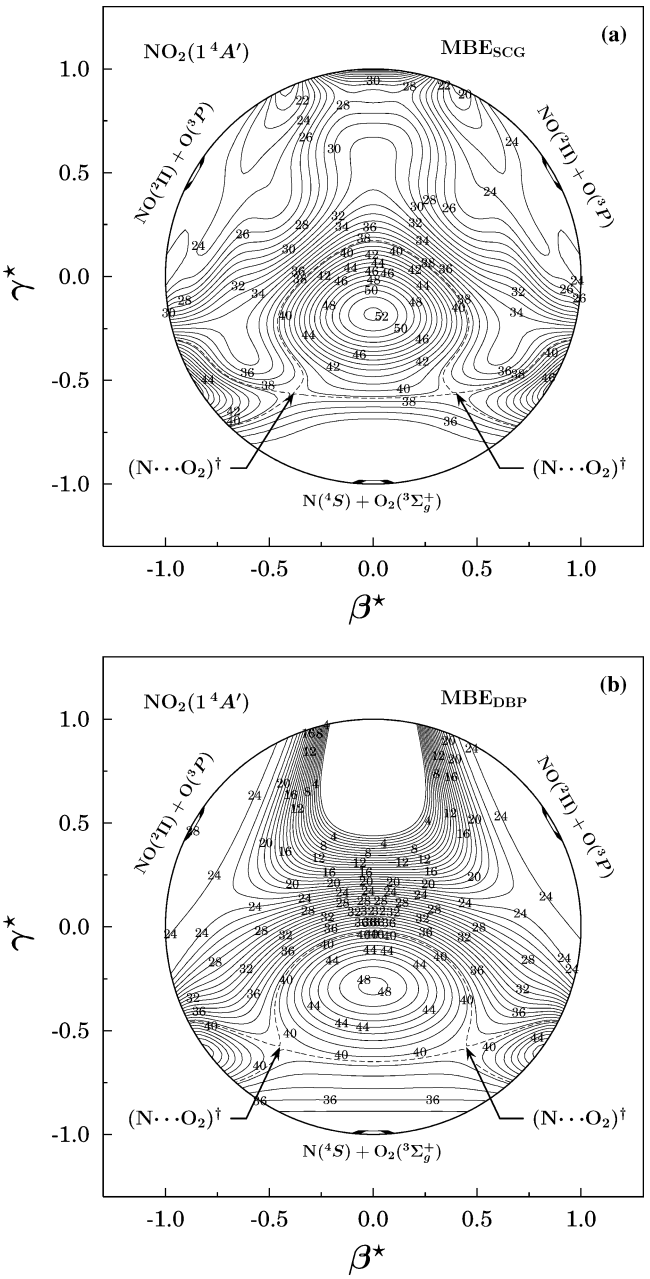

Figure 2. Relaxed triangular plot[45] for the MBE single-valued potential energy surfaces for the $1^4A'$ state of NO_2: (a) Duff et al.;[16,46] (b) Sayós et al.[20] The contours are the same as in Figure 1. Shown by the dashed line is the contour associated with the barrier height for the $N(^4S) + O_2$ reaction.

plots in panels a and b of Figure 2. The surface of Duff et al.[16,46] (MBE_{DBP}) was based on limited information from Walch and Jaffe[15] and hence is intended to be qualitative in areas not covered by the ab initio information. Thus, it should not be surprising that it displays a deep spurious well at C_{2v} geometries where the nitrogen atom gets between the two oxygen atoms, reaching an absolute minimum of $-0.48\ E_h$ (-13 eV) at a collinear geometry with $D_{\infty h}$ symmetry and a characteristic bond length of $R_{NO} = 2.190a_0$. Note that such an attribute has apparently no influence on the trajectory results, which may be explained by the fact that the insertion path has a high-energy ridge and the NO + O products channel samples only geometries with C_s symmetry. However, such a fortunate result might not have happened if quantum dynamics were employed for the calculations because of the possibility that the wave function may penetrate into such regions. The quartet potential energy surface of Sayós et al.[20] (MBE_{SCG}) also employs the MBE formalism, but the coefficients have been calibrated from a more extensive set of ab initio energies reported in their own work, leading to a function that is free from deep spurious wells. Such a surface shows two equivalent minima at $C_{\infty v}$ geometries ($R_{NO_a} = 2.227a_0$, $R_{NO_b} = 4.910a_0$, $R_{O_aO_b} = 7.137a_0$), which lie about 49.4 kcal mol^{-1} below the N + O_2 dissociation limit (16.7 kcal mol^{-1} below the NO + O dissociation limit), apparently not located in ref 20. Also visible is a small minimum with C_{2v} symmetry ($R_{NO_a} = R_{NO_b} = 2.507a_0$, $\angle O_aNO_b = 129.7°$), which is separated from the previous two minima by transition states with C_s symmetry. However, the most interesting feature from both surfaces is perhaps the high-energy ridge for the C_{2v} insertion of the nitrogen atom into O_2, which decreases as the nitrogen atom approaches the oxygen molecule along geometries with C_s symmetry. This feature bears some similarity with that encountered for the ground doublet surface, with the two equivalent barriers for the N + O_2 reaction now being located at C_s geometries and having barrier heights of 0.65 and 0.55 eV, respectively, for the MBE_{DBP} and MBE_{SCG} potential energy surfaces; see Table 1 for the harmonic vibrational frequencies. The potential energy surface of Sayós et al.[20] for $NO_2(^4A')$ shows an additional transition state close to the products chanel that lies approximately 33.3 kcal mol^{-1} below the N + O_2 dissociation limit (0.77 kcal mol^{-1} below the NO + O dissociation limit). The vibrational frequencies of this second saddle point are also given in Table 1, where we have characterized as symmetric stretching a mode that corresponds essentially to pure stretching of the short NO bond.

3. $N(^4S) + O_2$ Reaction

The dynamics study of reaction 1 on the lowest adiabatic sheet of $NO_2(^2A')$ has been carried out by using the QCT method. Because this method is widely described in the literature,[37,47,48] we summarize only the details most relevant to the present work. The thermal rate constant for the formation of NO + O assumes the general form

$$k(T) = g_e(T)\left(\frac{8k_BT}{\pi\mu_{N+O_2}}\right)^{1/2}\sum_{vj}\frac{(2j+1)\exp(-E_{vj}/k_BT)}{Q_{vj}} \times \int_0^\infty P(E_{tr})\,\sigma(E_{tr}, v, j)\,dE_{tr} \quad (5)$$

where $g_e(T) = {}^1/_6$ is the electronic degeneracy factor, k_B is the Boltzmann constant, E_{vj} is the rovibrational energy for the (v, j) state, Q_{vj} is the corresponding partition function, μ_{N+O_2} is the reduced mass of the reactants, and $\sigma(E_{tr}, v, j)$ is the reactive cross section. In turn, the integral in eq 5 represents the average reaction cross section, with the translational energy distribution being given by

$$P(E_{tr}) = \frac{E_{tr}}{(k_BT)^2}\exp\left(-\frac{E_{tr}}{k_BT}\right) \quad (6)$$

and normalized to unity for E_{tr} from 0 to ∞. To calculate the integral in eq 5, we may use a random sampling of E_{tr} from a Maxwell−Boltzmann distribution by the rejection method (ref 49 and references therein) or else[37] calculate the cumulative distribution function (CDF)

$$E_{tr} = -k_BT\ln(\xi_1\xi_2) \quad (7)$$

where ξ_1 and ξ_2 are two independent uniform random numbers. This approach is somewhat simpler than the former, having been adopted in the present work.

Similarly, the rovibrational states for a given temperature are obtained from a CDF as in ref 50, namely,

$$C^{vj}(E_{vj}) = \sum_{(v_0,j_0)}^{(v,j)} Q_{vj}^{-1}(2j+1)\exp(-E_{vj}/k_BT) \qquad (8)$$

where the summation runs over all allowed rovibrational states. Note that for the O_2 molecule, only odd rotational states are allowed starting from $j = 1$. The combination (v, j) for each trajectory is then obtained by minimizing $C(E_{vj}) - \xi_3 = 0$, where ξ_3 is a freshly generated uniform random number. Although in ref 50 this procedure has employed Morse curves to describe the diatomic molecule, we have chosen in this work a more realistic procedure by calculating the rovibrational energy from the numerical solution of the Schrödinger equation for the O_2 EHFACE2U[42] curve used to describe the diatomic in the DMBE/ES[21] potential energy surface. (Corresponding realistic forms have been used for the calculations on the $^4A'$ MBE surfaces.[16,20,46]) The internuclear distance for each rovibrational state has been calculated by the von Newman rejection method sampled between the turning points corresponding to the selected combination. Using the Monte Carlo method and the above sampling procedure, eq 5 reduces to

$$k(T) = g_e(T)\left(\frac{8k_BT}{\pi\mu_{N+O_2}}\right)^{1/2}\frac{N_r}{N}\pi b_{max}^2 \qquad (9)$$

where N_r is the number of reactive trajectories out of a set of N trajectories and b_{max} is the maximum impact parameter optimized from the standard procedure described in the literature. For statistical purposes, the estimated error of the rate constant is given by $\Delta k(T) = k(T)[(N - N_r)/NN_r]^{1/2}$.

3.1. Vibrational and Rotational Distributions of the NO Product. The vibrational distribution of the NO product molecules has been the subject of some controversy in the literature. Experimentally, there are reports of five measurements. Two of these were carried out by Whitson et al.[51] and Rahbee and Gibson[12] using first-overtone chemiluminescence. The others were by Herm et al.[13] utilizing laser-excited fluorescence, Winkler et al.[52] employing two-photon ionization, and most recently Caledonia et al.[14] using crossed beams. There is a notable variation in the measurements, particularly at the higher vibrational levels. Whereas three of the measurements[14,51,52] seem to suggest a preferential production of even over odd vibrational levels, the other two[12,13] show smoothly decreasing production with increasing vibrational level (possibly with a slight inversion at $v' = 1-2$).

To obtain nearly converged vibrational and rotational distributions, we have followed a strategy similar to that utilized in ref 30. Two sets ($v = 0$, 1) of 10 000 trajectories have then been calculated with 3.0 eV of translation energy, being the rotational quantum number obtained by the minimization of the rotational partition function for a temperature of 1000 K, namely, $C^{(v=0,1)j} - \xi = 0$ where $C^{(v=0,1)j}$ is given by eq 8 for a specific v state. Of course, such calculations have been performed both on the doublet[21] and quartet[16,20,46] spin state potential energy surfaces because both contribute under the chosen initial conditions according to $P_r = {}^2P_r + {}^4P_r$; ${}^\eta P_r$ is the reactive probability on the η-th spin state surface including the proper electronic degeneracy factor ($g_e = {}^1/_6$ for the doublet state and ${}^1/_3$ for the quartet state). Note that $T = 1000$ K has been chosen

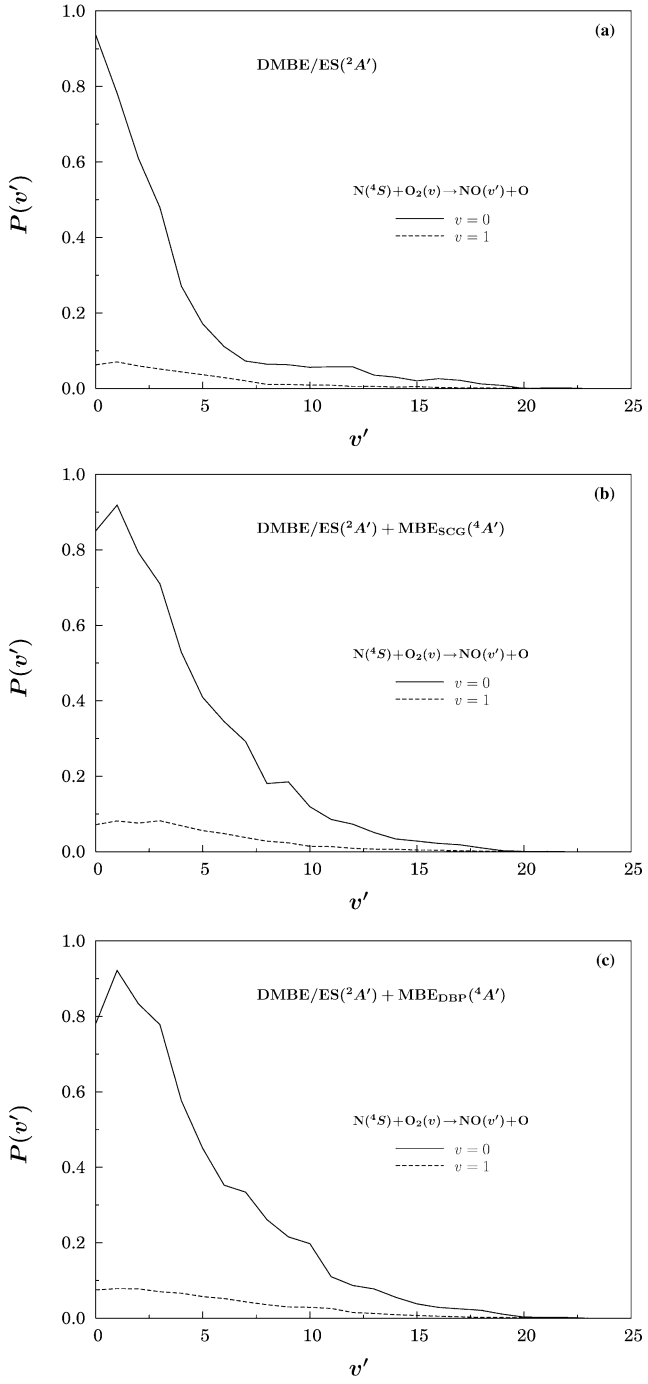

Figure 3. Product vibrational distribution for O_2 in vibrational states $v = 0$ and 1 at $E_{tr} = 3.0$ eV: (a) contribution of the $^2A'$ state as calculated from the DMBE/ES[21] potential energy surface; (b) total probability calculated using the DMBE/ES[21] and MBE$_{SCG}$[20] surfaces for the $^2A'$ and $^4A'$ states, respectively; (c) as in case b but using the MBE$_{DBP}$[16,46] surface for the quartet state of NO_2. The O_2 rotational temperature is assumed to be 1000 K. Both distributions are Boltzmann-weighted and normalized such that their sum peaks at unity.

to mimic the experimental conditions in the work of Caledonia et al.,[14] where the collisional velocity is 8 km s^{-1}. As pointed out in ref 30, although such a rotational temperature is probably higher than that observed under the experimental conditions, it may have the advantadge of being closer to the atmospheric situation. The product vibrational distributions so obtained are shown in panels a−c of Figure 3. Of them, panel a refers to the contribution obtained from the $^2A'$ state, and panels b and c show the probabilities when both the $^2A'$ and $^4A'$ states are considered. Note that the probabilities have been weighted by

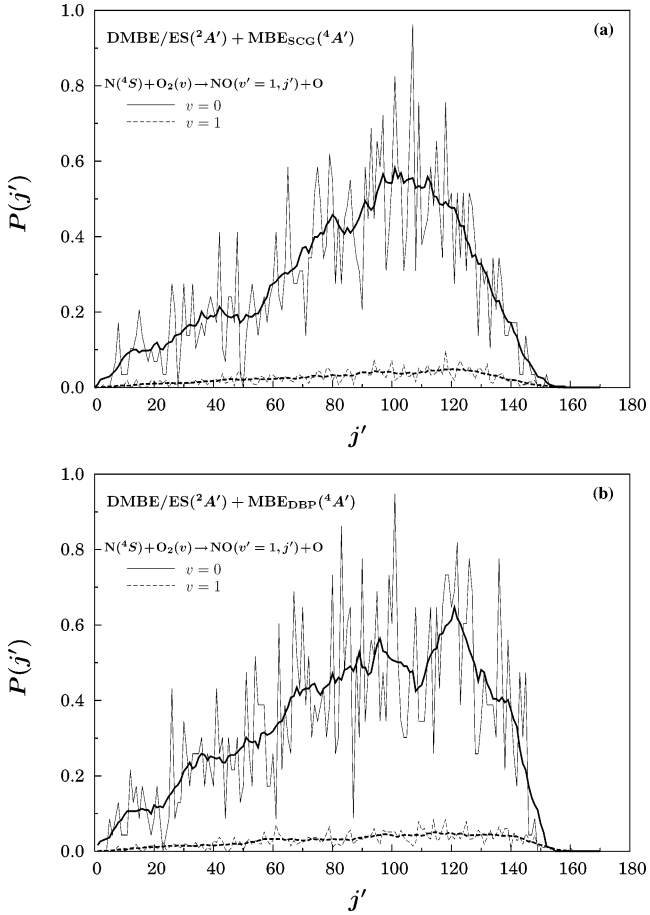

Figure 4. Product rotational distribution in NO($v' = 2$) from N + O_2($v = 0$, 1) at a collision energy of 3.0 eV: (a) distribution calculated using the DMBE/ES[21] and MBE_{SCG}[20] surfaces for the $^2A'$ and $^4A'$ states, respectively; (b) as in case a but using the MBE_{DBP}[16,46] surface for the quartet state of NO_2. The reactant rotational temperature is 1000 K. The thick lines represent smoothed distributions.

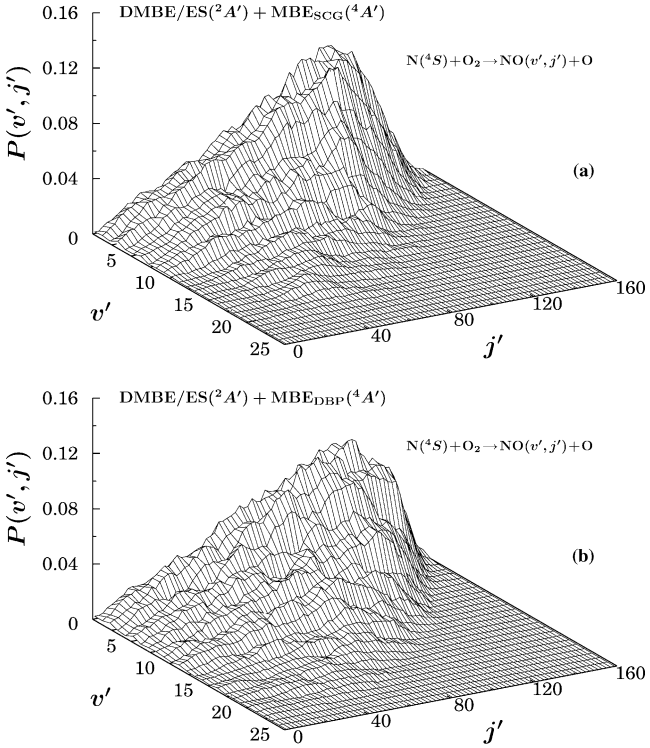

Figure 5. Product rovibrational distribution from N + O_2($v = 0$, 1) reactive collisions at a reactant rotational temperature of 1000 K. Panels are the same as in Figure 4.

the appropriate Boltzmann factor for $T = 1000$ K and hence cannot be directly compared with those reported in Figure 1 of ref 30, which have apparently not included such a weighting factor.[53] Note further that the calculated values are, within the statistical error, coincident with those obtained by sampling a thermalized distribution of v and j because the probability of getting populated states with $v \geq 2$ is rather small.

In turn, Figure 4 shows the corresponding product rotational distribution in NO($v' = 1$), which corresponds to the maximum in the v' distribution in Figure 3. As observed in ref 30, the large variations in the relative population of adjacent rotational levels may partly be due to incomplete convergence of the distributions. To smooth out such distributions, we have averaged neighboring rotational states by using standard smoothing procedures.[54] Specifically, we have used a moving-window averaging procedure (see ref 55 for the application of a similar procedure to the treatment of triatomic rotations) to mimic the smoothing caused by the proper treatment of the statistics, which consists of replacing each data value by an average of itself and six nearby neighbors, six to the left and six to the right. The curves (for $v = 0$, 1) resulting from such a smoothing are shown by the thick (solid and dashed, respectively) lines in Figure 4 for the case of $v' = 1$. In turn, the 2D plots of the Boltzmann weighted total probability for $v = 0$, 1, covering other values of v', are shown in Figure 5. Visible from both Figures 4 and 5 is the sharp drop off of the distributions at the high j' values, which is dictated by the fact that there is a limitation in the highest energetically accessible product rotational state for each vibrational manifold.[30]

In addition to the above vibrational-specific calculations, we have calculated a set of 10 000 trajectories with a similar translational energy but with the initial rovibrational distribution of the reactant oxygen molecule thermalized at 1000 K. As noted in the previous paragraph, besides the trajectories run on our DMBE/ES potential energy surface for the $^2A'$ state, similar calculations have been carried out using the MBE_{DBP} and MBE_{SCG} potential energy surfaces of NO_2($^4A'$) to obtain the proper averaged state values. The results so obtained are shown in Figure 6 and Table 2, which includes for comparison the trajectory results of Duff et al.[56] and Ramachandran et al.[30] (which are based on O_2($v = 0$, 1) alone). Although there are small variations depending on the quartet-state surface employed for the calculations, the results show common general trends. First, they indicate a small population inversion peaking at $v' = 1$, with product vibrational states populated to as much as $v' = 22$ in the case of using the $^4A'$ potential energy surface of Sayós et al.[20] and $v' = 23$ if the quartet-state surface is taken from Duff et al.[16,46] Apart from this, the shapes of both curves in Figure 6 are rather similar. The somewhat smaller cross sections reported for large v' values by Ramachandran et al.[30] can probably be attributed to the fact that the DMBE/ES[21] potential energy surface properly allows for sampling of the deep $^2A_1$ chemical well of NO_2, thus contrasting with the MBE surface[16] used by Ramachandran et al.[30] that shows erroneous behavior for such geometries. As a result, there is a small compensation manifested by a slight increase in the reactive probability for small v' values. This has been checked by analyzing all reactive trajectories run on DMBE/ES for the possible formation of a "complex". This has been defined as having been formed whenever a trajectory samples regions of configuration space lying at least 0.2 eV below the energy of the products channel. Such a region of configuration space is depicted in Figure 1 by the shaded area. Also shown for

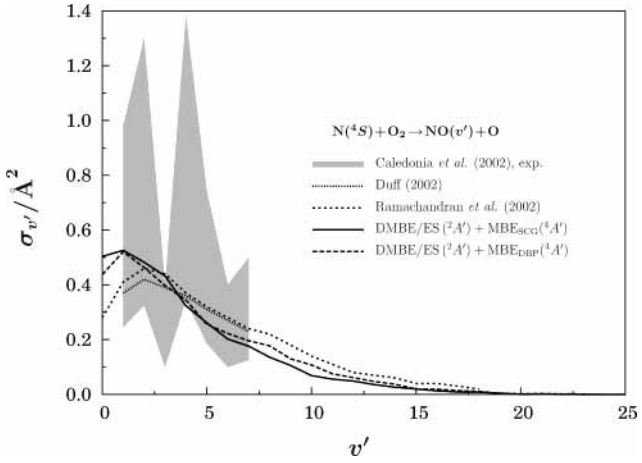

Figure 6. Comparison of the experimental[14] cross sections for N + $O_2(v) \rightarrow NO(v') + O$ with the results of the present calculations and those of Duff[56] and Ramachandran et al.[30] (The shaded area encompasses the error of a factor of 2 in the experimental results.[14]) (—) Results from the present study using the $^2A'$ DMBE/ES[21] and $^4A'$ MBE_{SCG}[20] surfaces. (— — —) Results from the present study using the $^2A'$ DMBE/ES[21] and $^4A'$ MBE_{DBP}[16,46] surfaces. The rovibrational distribution of O_2 is thermalized at $T = 1000$ K.

TABLE 2: Comparison of Calculated Cross Sections (in Å^2) for Selected v' States of Product NO Obtained at $E_{tr} = 3.0$ eV with Rovibrationally Thermalized O_2 Molecules at $T = 1000$ K with Theoretical[30,56] and Experimental[14] Results

v'	DMBE($^2A'$) + MBE_{DBP}($^4A'$)[a]	DMBE($^2A'$) + MBE_{SCG}($^4A'$)[b]	ref 14	ref 56	ref 30
0	0.43	0.50			0.28
1	0.52	0.53	0.49	0.37	0.41
2	0.46	0.48	0.65	0.42	0.46
3	0.40	0.43	0.20	0.39	0.44
4	0.34	0.32	0.69	0.36	0.37
5	0.26	0.26	0.37	0.31	0.32
6	0.22	0.20	0.20	0.27	0.28
7	0.20	0.18	0.25	0.27	0.24
8	0.18	0.14			0.22
9	0.13	0.11			0.18
10	0.11	0.07			0.14
11	0.08	0.06			0.11
12	0.06	0.05			0.08
13	0.05	0.04			0.07
14	0.04	0.03			0.06
15	0.02	0.02			0.04
16	0.02	0.01			0.04
17	0.01	0.01			0.03
18	0.01	0.01			0.02

[a] From this work, using the MBE_{DBP}[16] potential energy surface. [b] From this work, using the MBE_{SCG}[20] potential energy surface.

illustration are two reactive trajectories, one sampling the complex region and the other being direct and hence not sampling it. Statistically, we have calculated the probability of complex formation to be 24% of the total number of reactive trajectories, with the average complex lifetime being 1.61×10^{-14} s.

The second feature observed from Figure 6 refers to the fact that the results show hardly any evidence of oscillatory behavior on the v' dependence of the cross section. Such behavior contrasts with the experimental results of Caledonia et al.[14] while being in agreement with previous findings by Rahbee and Gibson[12] and Herm et al.[13] that suggest a smoothly decreasing production with increasing vibrational level, possibly with a slight population inversion for $v' = 1-2$ values. Despite such a disagreement with Caledonia et al.[14] on the oscillatory behavior of the cross-section dependence on v', our results fall within the error bars (the estimated error is a factor of 2, although a smaller error is attributed to relative values) of their measurements. They are also in good agreement both with the QCT calculations of Duff et al.[14] and Ramachandran et al.,[30] which employed MBE forms to represent both the $^2A'$ and $^4A'$ potential energy surfaces. Clearly, the uncertainty in the measurements is too large to descriminate among the various potential energy surfaces.

TABLE 3: Rotational Properties[a] for Selected v' States of Product NO Obtained at $E_{tr} = 3.0$ eV with Rovibrationally Thermalized O_2 at $T = 1000$ K

	DMBE($^2A'$) + MBE_{DBP}($^4A'$)[b]			DMBE($^2A'$) + MBE_{SCG}($^4A'$)[c]		
v'	j'_{max}	$\langle j' \rangle$	$\langle T_{rot} \rangle$/K	j'_{max}	$\langle j' \rangle$	$\langle T_{rot} \rangle$/K
0	151	107	27 656	151	100	24 172
1	150	103	25 373	148	100	23 923
2	151	102	24 627	146	98	22 742
3	145	99	22 962	145	95	21 153
4	138	96	21 370	138	92	19 635
5	134	95	20 705	132	87	17 381
6	129	92	19 214	127	85	16 416
7	139	90	18 190	139	80	14 392
8	130	85	16 056	125	77	13 192
9	118	84	15 507	118	76	12 709
10	118	79	13 570	112	72	11 286
11	121	78	13 080	108	68	9959
12	103	74	11 644	102	60	7679
13	105	72	10 898	101	65	8895
14	103	69	9896	103	55	6310
15	86	65	8684	86	57	6692
16	82	61	7562	82	49	4899
17	107	57	6529	107	49	4839
18	78	47	4400	78	52	5375

[a] Maximum rotational quantum number, average rotational quantum number, and rotational temperature. [b] From this work, using the MBE_{DBP}[16] potential energy surface. [c] From this work, using the MBE_{SCG}[20] potential energy surface.

Table 3 gathers the rotational properties of selected vibrational states of the NO product molecule. The average rotational temperature ($\langle T_{rot} \rangle \approx \langle E_{rot} \rangle / k_B$) was obtained from

$$\langle E_{rot} \rangle = B_{v'} \langle j' \rangle (\langle j' \rangle + 1) + D_{v'} [\langle j' \rangle (\langle j' \rangle + 1)]^2 \qquad (10)$$

where $\langle j' \rangle$ is the average rotational quantum number in the product NO molecule for a given v' state and the coefficients have their standard meaning:[57] $B_{v'} = B_e - \alpha_e(v' + 1/2)$, and $D_{v'} = D_e - \beta_e(v' + 1/2)$, with their numerical values being taken from the NIST Chemistry WebBook.[58] As seen from Table 3, the rotational temperatures cover the approximate ranges of $4000 \leq \langle T_{rot} \rangle / K \leq 28\,000$ and $5000 \leq \langle T_{rot} \rangle / K \leq 24\,000$ when using the MBE_{DBP}[16,46] and MBE_{SCG}[20] quartet-state forms in conjunction with the DMBE/ES[21] potential energy surface for the doublet state, respectively. The results generally agree with those of Ramachandran et al.,[30] which vary between 1200 and 34 000 K and hence basically encompass the range of 4000−10 000 K (this corresponds to $\langle j' \rangle = 40-64$) used by Caledonia et al.[14] in their spectral fits.

3.2. Thermalized Rate Constants. Table 4 reports the calculated rate constant for the title reaction. For the lowest adiabatic state of $NO_2(^2A')$, the calculations covered the temperature range between 1000 and 10 000 K, with a total of 3000 trajectories run per temperature, which minimizes the statistical error to about 10% at temperatures above 2000 K or so. (Such an error increases with decreasing temperature, reaching a value of about 30% at $T = 1000$ K.) As for the cross section, the total rate constant requires calculations on the potential energy surface for the $^4A'$ state because

$$k_1(T) = {}^2k_1(T) + {}^4k_1(T) \qquad (11)$$

TABLE 4: Parameters Used in the Present Calculations and Comparison of Rate Constant Results with the Values Recommended in the Literature[7] and the Variational Transition-State Results of Sayós et al.[20]

			$^2k_1$ (cm^3 s^{-1})		$k_1 = {}^2k_1 + {}^4k_1$ (cm^3 s^{-1})			
T/K	b_{max}/Å	N_r	this work	ref 20	$k_1{}^a$	$k_1{}^b$	VTST[20]	exptl[7]
300			1.75(−17)[c]	7.64(−17)	1.75(−17)	1.75(−17)	7.64(−17)	8.31(−17)
600			2.30(−14)[c]	2.97(−14)	2.30(−14)	2.34(−14)	3.01(−14)	3.87(−14)
1000	1.9	45	4.18(−13) ± 6.18(−13)	4.27(−13)	4.29(−13)	4.60(−13)	4.69(−13)	5.72(−13)
1250	2.3	96	1.46(−12) ± 1.47(−13)	1.02(−12)	1.52(−12)	1.64(−12)	1.20(−12)	1.37(−12)
1500	2.4	128	2.32(−12) ± 2.01(−13)	1.90(−12)	2.33(−12)	2.82(−12)	2.41(−12)	2.54(−12)
2000	2.3	285	5.48(−12) ± 3.37(−13)	4.38(−12)	6.39(−12)	7.37(−12)	6.27(−12)	5.85(−12)
3000	3.0	324	1.30(−11) ± 6.82(−13)	1.13(−11)	1.77(−12)	2.09(−11)	1.92(−11)	1.51(−11)
4000	3.1	471	2.33(−11) ± 9.85(−13)	1.95(−11)	3.48(−11)	4.08(−11)	3.70(−11)	2.65(−11)
5000	3.2	558	3.28(−11) ± 1.26(−12)	2.82(−11)	5.33(−11)	6.24(−11)	5.77(−11)	3.90(−11)
10 000	3.1	1006	7.87(−11) ± 2.02(−12)	8.14(−11)	1.64(−11)	1.93(−10)	2.54(−10)	

[a] Values of $^4k_1$ from ref 20 using VTST and the potential energy surface from Duff et al.[16] [b] Values of $^4k_1$ from ref 20 using VTST and the potential energy surface from the same reference. [c] Estimated values from eq 13.

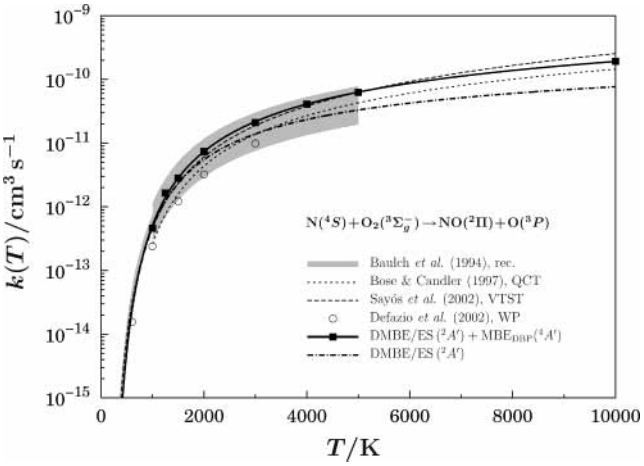

Figure 7. Total degeneracy averaged rate coefficients on the $^2A'$ and $^4A'$ potential energy surfaces as a function of temperature for the N + O_2 reaction. (−■−) From the present study using the QCT results on the $^2A'$ DMBE/ES[21] surface and the VTST results of Sayós et al.[20] on their own $^4A'$ surface. (− − −) VTST results of Sayós et al.[20] using their own $^2A'$ and $^4A'$ MBE surfaces.[21] (···) QCT results of Bose and Candler.[29] (○) Quantum wave packet results of Defazio et al.[36] The recommended values are indicated by the shaded area, which encompasses the associated error bars.[7]

where each contribution includes the appropriate electronic degeneracy factor; $^\eta k_1(T)$ is the total rate constant for the $^\eta A'$ ($\eta = 2, 4$) state. Such quartet-state calculations could be extracted from the literature[20] using both the potential energy surfaces of Duff et al.[16,46] and Soyos et al.[20] and hence were used directly as such; see Table 4.

Figure 7 shows the calculated values of the total rate constant and the corresponding Arrhenius equations (see later). For comparison with other theoretical calculations, we include the QCT results of Bose and Candler[29] based on the MBE surface of Duff et al.,[16] the variational transition-state theory (VTST) results of Sayós et al.[20] based on their own MBE form, and the quantum wave packet calculations of Defazio et al.[36] employing their most recent MBE surface. In addition, we present the rate constant recommended[7] by the CEC Group on Evaluation of Kinetic Data for Combustion Modelling established within the European Community Energy Research and Development Program. This is indicated as the gray shaded area, thus including the error bars for their recommended values.[7] Clearly, our results are in good agreement with the recommended values and are very close to the VTST values. In this case, our results show, for very high temperatures, a tendency to lower the rate constant because of opening of the atomization channel. (For $T = 10\,000$ K, the probability of dissociation into three atoms is about 1%.) For median temperatures (1250 to 1000 K), they slightly overestimate the VTST values. Such a slight underestimation relative to the VTST results for low-temperature regimes may be attributed both to differences in the potential energy surfaces used to represent the $NO_2(^2A')$ state and to quantum effects due to tunneling, which are included in VTST theory but not in the QCT method. In fact, although we are dealing with three heavy atoms, tunneling is by no means negligible for temperatures under 600 K. This may be rationalized by assuming a 1D Wigner barrier, where the transmission coefficient assumes the following temperature dependence:[59]

$$\kappa(T) = 1 + \frac{1}{24}\left[\frac{h\mathscr{F}(\nu^\dagger)}{k_B T}\right]^2 \tag{12}$$

where $\mathscr{F}(\nu^\dagger)$ denotes the absolute value of the imaginary frequency associated with the reaction coordinate; for the DMBE/ES[21] potential energy surface, $\nu^\dagger = 488.54\mathrm{i}\ \mathrm{cm}^{-1}$. From eq 12, we obtain $\kappa = 1.23$ for 300 K and 1.06 for 600 K. (For comparison, Sayós et al. reported $\kappa = 1.28$ for 300 K using their own potential energy surface.) Visible from Figure 7 is also the fact that wave packet calculations of Defazio et al.[36] underestimate the rate constant for all temperatures considered. As stated by the authors,[36] there are two main reasons that account for this discrepancy. The first is the impossibility of including all channels that are open at a given temperature, and the second concerns the barrier height of their MBE potential energy surface,[36] which, as they suggest, may overestimate by 0.56 kcal mol^{-1} the true barrier height. Note also the differences between our results and those of Bose and Candler,[29] which are likely to be associated with the different potential energy surfaces used for the calculations as well as the sampling procedure of initial conditions.

The temperature dependence of the calculated rate constants can be modeled by a three-parameter Arrhenius equation

$$^\eta k_1(T) = AT^n \exp\left(-\frac{B}{T}\right) \tag{13}$$

with the optimum least-squares parameters obtained from the present work for the doublet $^2A'$ surface ($\eta = 2$) being $A = 3.40 \times 10^{-13}$ cm^3 s^{-1} K^{-n}, $n = 0.63$, and $B = 4043.29$ K. Similarly, one has $A = 2.31 \times 10^{-14}$ cm^3 s^{-1} K^{-n}, $n = 0.97$, and $B = 7458.75$ K for the quartet-state results of Duff et al.;[16] $A = 1.41 \times 10^{-14}$ cm^3 s^{-1} K^{-n}, $n = 1.04$, and $B = 6112.00$ K for the quartet-state results of Soyos et al.[20] Both sets of parameters were obtained from a least-squares fitting procedure to VTST results.[20] Note that the rate constant for this reaction is quite small up to temperatures of about $T = 3000$ K, and hence it would be rather expensive to obtain converged results

by running classical trajectories. Using the results based on the Duff et al.[16] potential function for the $^4A'$ state, we then predict the total rate constant to be 2.30(2.44) $\times$ 10^{-14} cm^3 s^{-1} and 1.76 (2.16) $\times$ 10^{-17} cm^3 s^{-1} for T = 600 and 300 K, respectively. (Given in parentheses are the values corrected with the 1D tunneling transmission coefficients.) Similarly, from the Sayós et al.[20] results for the $^4A'$ state, we predict the total rate constant to be 2.34(2.48) $\times$ 10^{-14} cm^3 s^{-1} and 1.76 (2.16) $\times$ 10^{-17} cm^3 s^{-1} for T = 600 and 300 K, respectively. Both of the above predictions are seen to underestimate slightly the results reported in ref 20. Note also that for low temperatures where the electronic doublet state should dominate our estimates obtained from a simple extrapolation of the Arrhenius equation slightly underestimate the recommended results of Baulch et al.[7] Besides extrapolation errors, this may be attributed also to the fact that quantum effects such as tuneling are ignored in the QCT method.

4. O + NO Reaction

To study the O + NO reaction, we have adopted a different strategy. As the literature[7] shows, the thermalized rate constant for this endoergic reaction assumes values ranging from 1.28 $\times$ 10^{-20} cm^3 s^{-1} at 1000 K to 3.71 $\times$ 10^{-13} cm^3 s^{-1} at 5000 K. Even for the latter, the use of the QCT method becomes computationally very demanding for giving converged reactive cross sections. (The probability of finding a reactive trajectory is about 1 in 10 000.) To overcome this difficulty, we have chosen to calculate the O + NO rate constant by assuming the microreversibility principle, which implies that the rate for this reaction can be estimated from that for the direct N(^4S) + O_2 reaction and the corresponding equilibrium constant, on which we focus next.

Let us consider the equilibrium

$$N(^4S) + O_2(X^3\Sigma_g^-) \rightleftarrows NO(X\,^2\Pi) + O(^3P) \qquad (14)$$

where the equilibrium constant is defined by

$$K(T) = \frac{k_1(T)}{k_{-1}(T)} \qquad (15)$$

with k_1 being the total rate constant for the direct reaction, eq 11, and k_{-1} being the total rate constant for its reverse. Because $k_1(T)$ has been calculated in section 3.2, the key quantity missing to calculate $k_{-1}(T)$ by using eq 15 is the equilibrium constant. This can be determined from statistical thermodynamics as

$$K(T) = \frac{Q_{ele}^{O(^3P)} Q_{ele}^{NO(^2\Pi)}}{Q_{ele}^{N(^4S)} Q_{ele}^{O_2(^3\Sigma_g^-)}} \left(\frac{\mu_{O+NO}}{\mu_{N+O_2}}\right)^{3/2} \times \frac{\sum_{v,j}^{NO} (2j+1)\exp(-E_{vj}/k_B T)}{\sum_{v,j}^{O_2} (2j+1)\exp(-E_{vj}/k_B T)} \exp\left(-\frac{\Delta E}{k_B T}\right) \qquad (16)$$

where μ_i is the reduced mass and ΔE is the energy difference between the reactants and products. Note that the summation in v, j runs over the total number of states available; for NO($^2\Pi$), all rotational states count starting at j = 1, whereas for $O_2(X\,^3\Sigma_g^-)$ only odd rotational states starting at j = 1 contribute. In turn, the electronic partition functions Q_{ele}^x for the N(^4S) atom and O_2 molecule correspond to their spin multiplicities, namely, $Q_{ele}^{N(^4S)} = 4$ and $Q_{ele}^{O_2(^3\Sigma_g^-)} = 3$. For O($^3P$) and NO($^2\Pi$), we need to take into account spin−orbit interactions, with the electronic partition functions assuming the forms

$$Q_{ele}^{O(^3P)} = 5 + 3\exp(-227.7/T) + \exp(-326.6/T) \qquad (17)$$

$$Q_{ele}^{NO(^2\Pi)} = 2 + 2\exp(-174.2/T) \qquad (18)$$

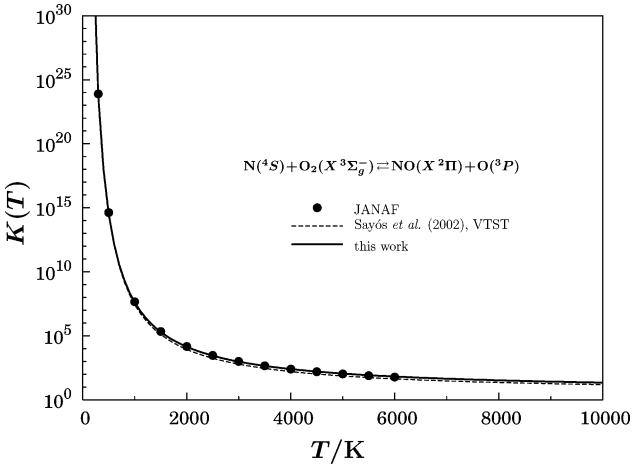

Figure 8. Equilibrium constant. (—) Statistical thermodynamics results calculated in this work from eqs 15 and 16. (− − −) Results calculated from the VTST rate constants of Sayós et al.[20] for the direct and reverse reaction. (●) Values from JANAF[60] tables.

Figure 8 shows the dependence of the calculated equilibrium constant on temperature. Also shown for comparison are the results obtained from the JANAF[60] tables and those calculated from the VTST total rate constants of Sayós et al.[20] for the forward and reverse reactions. Clearly, the statistical thermodynamics results show, over 30 orders of magnitude, excellent agreement with the JANAF results. Although the values estimated from the VTST total rate constants[20] slightly underestimate the JANAF values, the agreement with the latter is also seen to be good.

The temperature dependence of the NO + O total rate constant, $k_{-1} = k_1/K$, is shown in Figure 9 by the solid line, and the dash line indicates the VTST results of Sayós et al.[20] As in Figure 7, the shaded area delimits the error bars of the recommended values:[7] $k_{-1} = 1.14 \times 10^{-15} T^{1.13} \exp(-19\,200/T)$ with $\Delta \log k = \pm 0.30$ up to 5000 K. Clearly, the agreement with both the latter and the VTST results[20] is good.

5. Conclusions

In this work, we have used the lowest adiabatic sheet of a previously reported DMBE/ES[21] form for the $^2A'$ electronic manifold of NO_2 to calculate the corresponding contribution to the dynamics and kinetics of the N(^4S) + O_2 reaction. The focus has been on the rovibrational distributions of the NO product molecule at a collisional energy of 3 eV and the temperature dependence of the total rate constant. The quartet-state ($^4A'$) contribution to the dynamics attributes has been obtained from results that are available in the literature[20] or else calculated using single-sheeted MBE potentials from various sources.[16,20,46] In turn, the total rate constant for the O + NO reaction has been determined from the calculated equilibrium constant and the rate constant for the N(^4S) + O_2 reaction. The agreement with the recommended rate constants is good, and the rovibrational distributions of NO are found to be similar to other reported theoretical estimates.[30,56] In fact, although failing to

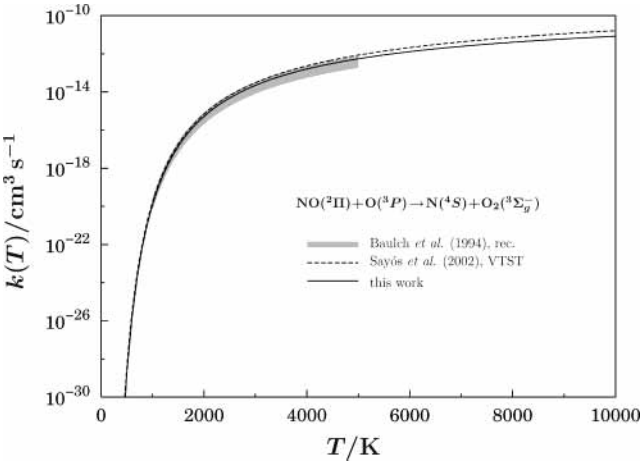

Figure 9. Total degeneracy averaged rate coefficients on the $^2A'$ and $^4A'$ potential energy surfaces as a function of temperature for the O + NO reaction. (—) Results from the present study using the equilibrium constant and the total rate constant for the direct reaction based on the $^2A'$ DMBE/ES[21] and the $^4A'$ MBE_{SCG}[20] surfaces. (— — —) VTST results of Sayós et al.[20] The recommended results and corresponding error bars are indicated by the shaded area.[7]

show any oscillatory structure, as earlier experimental results[12,13] suggest, our results show fair agreement with the general trends actually observed from recent crossed-beam experiments.[14] Despite the contribution of the quartet-state surface, the results therefore suggest that the $^2A'$ DMBE/ES potential energy surface is also recommended for accurate dynamics studies of the N(^4S) + O_2 reaction and its reverse. Of course, further theoretical and experimental work is required to clarify the points of disagreement in the vibrational dependence of the product NO molecule.

Acknowledgment. We thank Jim Duff (SRI, Massachussets) for providing the code for the potential energy surface in ref 16 and Naduvala Balakrishnan (University of Nevada, Las Vegas) for helpful correspondence. This work has the support of Fundação para a Ciência e a Tecnologia, Portugal, via project POCTI/40154/QUI/2001, and FEDER.

References and Notes

(1) Wayne, R. P. *Chemistry of Atmospheres;* Oxford University Press: Oxford, England, 2002.
(2) Sharma, R. D.; Sun, Y.; Dalgarno, A. *Geophys. Res. Lett.* **1993**, *20*, 2043.
(3) Sharma, R. D.; von Esse, H. D. F.; Kharchenko, V. A.; Sun, Y.; Dalgarno, A. *J. Geophys. Res.* **1996**, *101*, 19707.
(4) Hubert, B.; Gerard, J.; Shematovich, V. I.; Bisikalo, D. V. *Geophys. Res. Lett.* **1996**, *23*, 2215.
(5) Duff, J. W.; Sharma, R. D. *J. Chem. Soc., Faraday Trans.* **1997**, *93*, 2645.
(6) Zeldovich, Y. B.; Sadovnikov, P. Y.; Frank-Kamenetskii, D. A. *Oxidation of Nitrogen in Combustion*; Technical Report; Academy of Sciences of the URSS, Institute of Physics: Moscow-Leningrad, 1947.
(7) Baulch, D. L.; Cobos, C. J.; Cox, R. A.; Hayman, G.; Just, T.; Kerr, J. A.; Murrells, T.; Pilling, M. J.; Troe, J.; Walker, R. W.; Warnatz, J. *J. Phys. Chem. Ref. Data* **1994**, *23*, 873.
(8) Swaminathan, P. K.; Strobel, D. F.; Kupperman, D. G.; Krishna Kumar, C.; Acton, L.; DeMajistre, R.; Yee, J.; Paxton, L.; Anderson, D. E.; Strickland, D. J.; Duff, J. W. *J. Geophys. Res.* **1998**, *103*, 11579.
(9) Balakrishnan, N.; Sergueeva, E.; Kharchenko, K.; Dalgarno, A. *J. Geophys. Res.* **2000**, *105*, 18549.
(10) Gerard, J. C.; Shamotovic, V. I.; Bisikalo, D. V. *Geophys. Res. Lett.* **1991**, *18*, 1695.
(11) Lie-Svendsen, O.; Rees, M. H.; Stamnes, K.; Whipple, E. C., Jr. *Planet. Space Sci.* **1991**, *39*, 929.
(12) Rahbee, A.; Gibson, J. J. *J. Chem. Phys.* **1981**, *74*, 5143.
(13) Herm, R. R.; Sullivan, B. J.; Whitson, M. E., Jr. *J. Chem. Phys.* **1983**, *79*, 2221.
(14) Caledonia, G. E.; Krech, R. H.; Oakes, D. B.; Lipson, S. J.; Blumberg, W. A. M. *J. Geophys. Res.* **2000**, *105*, 12833.
(15) Walch, S. P.; Jaffe, R. L. *J. Chem. Phys.* **1987**, *86*, 6946.
(16) Duff, J. W.; Bien, F.; Paulsen, D. E. *Geophys. Res. Lett.* **1994**, *21*, 2043.
(17) Murrell, J. N.; Carter, S.; Farantos, S. C.; Huxley, P.; Varandas, A. J. C. *Molecular Potential Energy Functions*; Wiley: Chichester, England, 1984.
(18) Sayós, R.; Oliva, C.; González, M. *J. Chem. Phys.* **2001**, *115*, 1287.
(19) González, M.; Oliva, C.; Sayós, R. *J. Chem. Phys.* **2002**, *117*, 680.
(20) Sayós, R.; Oliva, C.; González, M. *J. Chem. Phys.* **2002**, *117*, 670.
(21) Varandas, A. J. C. *J. Chem. Phys.* **2003**, *119*, 2596.
(22) Varandas, A. J. C.; Voronin, A. I. *Mol. Phys.* **1995**, *95*, 497.
(23) Varandas, A. J. C. *Lecture Notes in Chemistry*; Laganá, A., Riganelli, A., Eds.; Springer: Berlin, 2000; Vol. 75, p 33.
(24) Varandas, A. J. C. *Conical Intersections: Electronic Structure, Dynamics and Spectroscopy*; Yarkony, D., Köppel, H., Domcke, W., Eds.; World Scientific Publishing: Singapore, 2004.
(25) Varandas, A. J. C. *J. Chem. Phys.* **1996**, *105*, 3524.
(26) Gilibert, M.; Aguilar, A.; González, M.; Sayós, R. *Chem. Phys.* **1993**, *172*, 99.
(27) Gilibert, M.; Aguilar, A.; González, M.; Sayós, R. *Chem. Phys.* **1993**, *178*, 287.
(28) Sayós, R.; Aguilar, A.; Gilibert, M.; González, M. *J. Chem. Soc., Faraday Trans.* **1993**, *89*, 3223.
(29) Bose, D.; Candler, G. V. *J. Chem. Phys.* **1997**, *107*, 6136.
(30) Ramachandran, R.; Balakrishnan, N.; Dalgarno, A. *Chem. Phys. Lett.* **2000**, *331*, 562.
(31) Valli, G. S.; Orru, R.; Clementi, E.; Laganá, A.; Crocchianti, S. *J. Chem. Phys.* **1995**, *102*, 2825.
(32) Sayós, R.; Hijazo, J.; Gilibert, M.; González, M. *Chem. Phys. Lett.* **1998**, *284*, 101.
(33) Gilibert, M.; Gimenez, X.; González, M.; Sayós, R.; Aguilar, A. *Chem. Phys.* **1995**, *191*, 1.
(34) Balakrishnan, N.; Dalgarno, A. *Chem. Phys. Lett.* **1999**, *302*, 485.
(35) Defazio, P.; Gray, S. K.; Petrongolo, C.; Oliva, C. *J. Chem. Phys.* **2001**, *115*, 3208.
(36) Defazio, P.; Petrongolo, C.; Oliva, C.; González, M.; Sayós, R. *J. Chem. Phys.* **2002**, *117*, 3647.
(37) Peslherbe, G. H.; Wang, H.; Hase, W. L. *Adv. Chem. Phys.* **1999**, *105*, 171.
(38) Hase, W. L.; Duchovic, R. J.; Hu, X.; Komornicki, A.; Lim, K. F.; Lu, D.; Peslherbe, G. H.; Swamy, K. N.; Linde, S. R. V.; Varandas, A. J. C.; Wang, H.; Wolf, R. J. *QCPE Bull.* **1996**, *16*, 43.
(39) Kuntz, P. J. *Dynamics of Molecular Collisions*, part B; Miller, W., Ed.; Modern Theoretical Chemistry; Plenum: New York, 1976; p 53.
(40) Tully, J. C. *Adv. Chem. Phys.* **1980**, *42*, 63.
(41) Varandas, A. J. C.; Silva, J. D. *J. Chem. Soc., Faraday Trans. 2* **1986**, *82*, 593.
(42) Varandas, A. J. C.; Silva, J. D. *J. Chem. Soc., Faraday Trans.* **1992**, *88*, 941.
(43) Schryber, J. H.; Polyansky, O. L.; Jensen, P.; Tennyson, J. *J. Mol. Spectrosc.* **1997**, *185*, 234.
(44) Varandas, A. J. C. *J. Chem. Phys.* **1997**, *107*, 867.
(45) Varandas, A. J. C. *Chem. Phys. Lett.* **1987**, *138*, 455.
(46) Duff, J. W. Private communication, February 2003.
(47) Bunker, D. L. *Methods Comput. Phys.* **1971**, *10*, 287.
(48) Porter, R. N.; Raff, L. M. In *Dynamics of Molecular Collisions*, part B; Miller, W. H., Ed.; Modern Theoretical Chemistry; Plenum: New York, 1976; Vol. 2, p 1.
(49) Varandas, A. J. C.; Brandão, J.; Pastrana, M. R. *J. Chem. Phys.* **1992**, *96*, 5137.
(50) Rodrigues, S. P. J.; Varandas, A. J. C. *J. Phys. Chem. A* **2003**, *107*, 5369.
(51) Whitson, M. E., Jr.; Darnton, L. A.; McNeal, R. *Chem. Phys. Lett.* **1976**, *41*, 552.
(52) Winkler, I. C.; Stachnik, R. A.; Steinfeld, J. I.; Miller, S. M. *J. Chem. Phys.* **1986**, *85*, 890.
(53) Balakrishnan, N. Private communication, September 2003.
(54) Press, W. H.; Teukolsky, S. A.; Vetterling, W. T.; Flannery, B. P. *Numerical Recipes in Fortran: The Art of Scientific Computing;* Cambridge University Press: New York, 1992.
(55) Varandas, A. J. C. *Mol. Phys.* **1995**, *85*, 1159.
(56) Duff, J. W., cited in ref 14.
(57) Huber, K. P.; Herzberg, G. *Molecular Spectra and Molecular Structure*. Van Nostrand: New York, 1979; Vol. 4 (Constants of Diatomic Molecules).
(58) *NIST Chemistry WebBook* **2003**, *69*, http://webbook.nist.gov/chemistry.
(59) Wigner, E. *Z. Phys. Chem. B* **1932**, *19*, 203.
(60) Chase, M. W., Jr.; Davies, C. A.; Downey, J. R., Jr.; Frurip, D. J.; McDonald, R. A.; Syveraud, A. N. *JANAF Thermodynamic Tables*, 3rd ed.; American Chemical Society and American Institute for Physics for the National Bureau of Standards: Washington, DC, New York, 1985.